Neutrino factory for both large and small θ_{13}

Alan Bross, Malcolm Ellis, and Steve Geer*
Fermi National Accelerator Laboratory, Batavia, Illinois 60510-0500, USA

Olga Mena+
INFN-Sezione di Roma, Dipartimento di Fisica, Universitá di Roma "La Sapienza," Piazzale Aldo Moro, 5, I-00185 Roma, Italy

Silvia Pascoli‡
IPPP, Department of Physics, Durham University, Durham DH1 3LE, United Kingdom
(Received 4 October 2007; published 28 May 2008)

An analysis of the neutrino oscillation physics capability of a low-energy neutrino factory is presented, including a first simulation of the detector efficiency and event energy threshold. The sensitivity of the physics reach to the presence of backgrounds is also studied. We consider a representative baseline of 1480 km, we use muons with 4.12 GeV energy and we exploit a very conservative estimate of the energy resolution of the detector. Our analysis suggests an impressive physics reach for this setup, which can eliminate degenerate solutions, for both large and small values of the mixing angle θ_{13}, and can determine leptonic CP violation and the neutrino mass hierarchy with extraordinary sensitivity.

DOI: 10.1103/PhysRevD.77.093012 PACS numbers: 14.60.Pq

I. INTRODUCTION

In recent years compelling evidence for neutrino oscillations has been found in experiments with atmospheric [1], solar [2–7], reactor [8] and long-baseline accelerator neutrinos [9,10]. Two mass squared differences, $\Delta m_{ji}^2 \equiv m_j^2 - m_i^2$, have been measured with good accuracy, their present best fit values being $|\Delta m_{31}^2| = 2.5 \times 10^{-3}$ eV^2 and $|\Delta m_{21}^2| = 8.0 \times 10^{-5}$ eV^2. In addition, explaining the experimental data in terms of neutrino oscillations requires two large mixing angles in the leptonic mixing matrix U. Their best fit values are $\sin^2\theta_{12} = 0.30$ and $\sin^2 2\theta_{23} = 1$, see Refs. [11–13]. Despite the remarkable recent progress in our understanding of neutrino physics, fundamental questions remain unanswered. It is crucial to establish the nature of neutrinos—whether they are Dirac or Majorana particles, the neutrino mass ordering, the absolute neutrino mass scale, the value of the unknown mixing angle θ_{13}, the presence or absence of CP violation in the leptonic sector, and the precise values of the already known oscillation parameters. This information will help shed light on the physics beyond the standard model responsible for neutrino masses and for the leptonic mixing structure.

In order to achieve these goals, very sensitive neutrino experiments will be required. In particular, long-baseline oscillation experiments are expected to play an important role in providing precision measurements of the neutrino oscillation parameters, the CP-violating phase δ, and a determination of the neutrino mass ordering.

Neutrino factories [14], in which a neutrino beam is generated from muons decaying within the straight sections of a storage ring, have been studied extensively in the past, and have been shown to be sensitive tools for studying neutrino oscillation physics [14–27]. In a neutrino factory far detector, the experimental signature for the so-called *golden channel* [18] is the presence of a *wrong-sign* muon [14,15], i.e. a muon with opposite sign to the muons stored in the neutrino factory. Wrong-sign muons result from $\nu_e \to \nu_\mu$ oscillations, and can be used to measure the unknown mixing angle θ_{13}, determine the neutrino mass hierarchy, and search for CP violation in the neutrino sector. This physics program requires the detection of charged current (CC) muon-neutrino interactions, and the measurement of the sign of the produced muon. If the interacting neutrinos have energies of more than a few GeV, standard neutrino detector technology, based on large magnetized sampling calorimeters, can be used to measure wrong-sign muons with high efficiency and very low backgrounds. This has been shown to work for neutrino factories with energies of about 20 GeV or greater [18,21,28].

Lower energy neutrino factories [26], which store muons with energies <10 GeV, require a detector technology that can detect lower energy muons. Recently ideas have emerged for a neutrino factory detector based on a fully active calorimeter within a potentially affordable large volume magnet. These ideas encourage consideration of low-energy neutrino factories. Initial studies [26], based on a first guess for the performance of a low-energy neutrino factory detector, suggested that a neutrino factory with an energy of about 4 GeV would enable very precise measurements of the neutrino mixing parameters. In the present paper, we consider in more detail the expected

*sgeer@fnal.gov
+omena@fnal.gov
‡silvia.pascoli@durham.ac.uk

performance of a low-energy neutrino factory detector, and update and extend our previous studies to include a more realistic detector model and a more comprehensive study of systematic effects. In particular we exploit the low-energy threshold of the detector and make a very conservative estimate for its energy resolution which, together with the broad spectrum of the neutrino factory beam, facilitates the elimination of degeneracies [29–32]. It is well known that even a very precise measurement of the appearance probability for neutrinos and antineutrinos at a fixed L/E allows different solutions for $(\theta_{13}, \mathrm{sgn}(\Delta m^2_{13}), \delta)$, weakening severely the sensitivity to these parameters. Many strategies have been advocated to resolve this issue which in general involve another detector [20,33–38] or the combination with another experiment [24,25,39–48]. Using the energy dependence of the signal in the low-energy neutrino factory, we find that a 4 GeV neutrino factory can unambiguously determine all of the neutrino oscillation parameters with good precision provided $\sin^2 2\theta_{13} > \text{few} \times 10^{-3}$. Hence a low-energy neutrino factory would be a precision tool for both large and small θ_{13}.

In Sec. II we describe the design for the low-threshold detector and its performance. In Sec. III, we discuss in detail the physics reach of the proposed setup. We first consider the disappearance ν_μ signal in order to determine precisely the value of the atmospheric mass squared difference and, possibly, the type of hierarchy even for $\theta_{13} = 0$. Then, we consider the appearance signals $\nu_e \to \nu_\mu$ and $\bar{\nu}_e \to \bar{\nu}_\mu$, which depend on θ_{13}, δ and the type of neutrino mass ordering. We perform a detailed numerical simulation and discuss the sensitivity of the low-energy neutrino factory to these parameters. In Sec. IV, we draw our conclusions.

II. DETECTOR DESIGN AND PERFORMANCE

A totally active scintillator detector (TASD) has been proposed for a neutrino factory, and results from a first study of its expected performance are described in the recent International Scoping Study Report [28]. Using a TASD for neutrino physics is not new. Examples are KamLAND [8], which has been operating for several years, and the proposed NOνA detector [49], which is a 15–18 kton liquid scintillator detector that will operate off axis to the NuMI beam line [50] at Fermilab. Note that, unlike KamLAND or NOνA, the TASD we are investigating for the low-energy neutrino factory is magnetized and has a segmentation that is approximately 10 times that of NOνA. Magnetization of such a large volume ($> 30\,000\ \mathrm{m}^3$) is the main technical challenge in designing a TASD for a neutrino factory, although research and development to reduce the detector cost (driven in part by the large channel count, 7.5×10^6) is also needed.

The neutrino factory TASD we are considering consists of long plastic scintillator bars with a triangular cross section arranged in planes which make x and y measurements (we plan to also consider an x-u-v readout scheme). Optimization of the cell cross section still needs further study since a true triangular cross section results in tracking anomalies at the corners of the triangle. The scintillator bars have a length of 15 m and the triangular cross section has a base of 3 cm and a height of 1.5 cm. We have considered a design using liquid as in NOνA, but, compared to NOνA, the cell size is small (NOνA uses a $4 \times 6\ \mathrm{cm}^2$ cell) and the nonactive component due to the polyvinyl chloride extrusions that hold the liquid becomes quite large (in NOνA, the scintillator is approximately 70% of the detector mass). Our design is an extrapolation of the MINERνA experiment [51] which in turn was an extrapolation of the D0 preshower detectors [52]. We are considering a detector mass of approximately 35 kton (dimensions $15 \times 15 \times 150$ m). We believe that an air-core solenoid can produce the field required (0.5 T) to do the physics.

As was mentioned above, magnetizing the large detector volume presents the main technical challenge for a neutrino factory TASD. Conventional room temperature magnets are ruled out due to their prohibitive power consumption, and conventional superconducting magnets are believed to be too expensive, due to the cost of the enormous cryostats needed in a conventional superconducting magnet design. In order to eliminate the cryostat, we have investigated a concept based on the superconducting transmission line (STL) that was developed for the Very Large Hadron Collider (VLHC) superferric magnets [53]. The solenoid windings now consist of this superconducting cable which is confined in its own cryostat (Fig. 1). Each solenoid (10 required for the full detector) consists of 150 turns and requires 7500 m of cable. There is no large vacuum vessel and thus no large vacuum loads which make the cryostats for large conventional superconducting magnets very expensive.

The neutrino factory TASD response has been simulated with GEANT4 version 8.1 (Fig. 2). The GEANT4 model of the

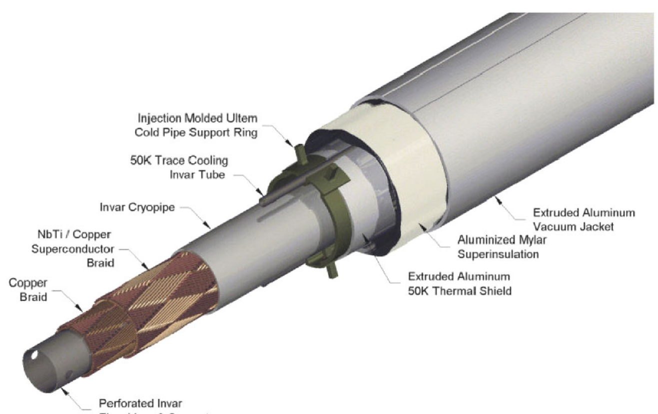

FIG. 1 (color online). Diagram of superconducting transmission line design.

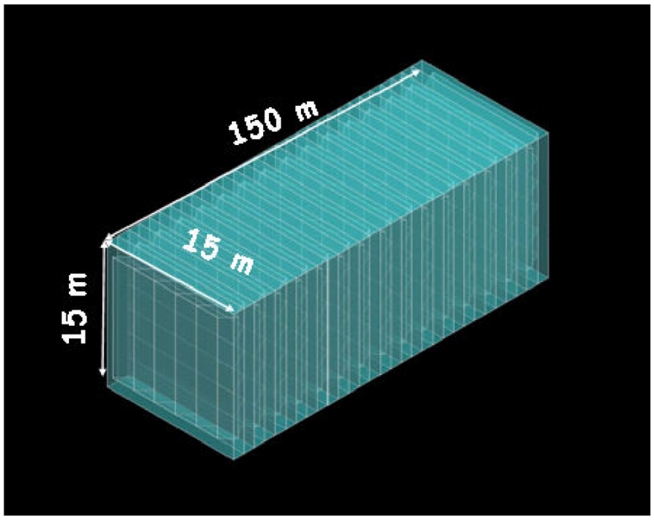

FIG. 2 (color online). Schematic of totally active scintillator detector.

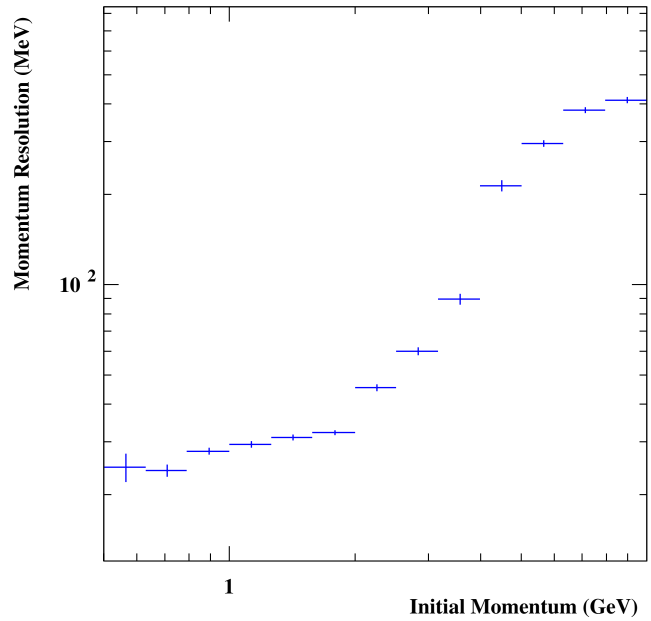

FIG. 3 (color online). Momentum resolution as a function of the muon momentum.

detector included each of the individual scintillator bars, but did not include edge effects on light collection, or the effects of a central wavelength shifting fiber. A uniform 0.5 T magnetic field was simulated.

Samples of isolated muons in the range of momentum between 100 MeV/c and 15 GeV/c were simulated to allow the determination of the momentum resolution and charge identification (ID) capabilities. The NUANCE [54] event generator was also used to simulate 1×10^6 ν_e and 1×10^6 ν_μ interactions. Events were generated in 50 monoenergetic neutrino energy bins between 100 MeV and 5 GeV. The results that follow only have 1000 events processed through the GEANT4 simulation and reconstruction.

The detector response was simulated assuming a light yield consistent with MINERνA measurements and current photodetector performance [49]. In addition, a 2 photoelectron energy resolution was added through Gaussian smearing to ensure that the energy resolution used in the following physics analysis would be a worst-case estimate. Since a complete pattern recognition algorithm was beyond the scope of our study, for our analysis the Monte Carlo information was used to aid in pattern recognition. All digitized hits from a given simulated particle where the reconstructed signal was above 0.5 photoelectrons were collected. When using the isolated particles, hits in neighboring x and y planes were used to determine the 3-dimensional position of the particle. The position resolution was found to be approximately 4.5 mm rms with a central Gaussian of width 2.5 mm.[1] These space points were then passed to the RECPACK KALMAN track fitting package [55].

[1]At this stage, the simulation does not take into account light collection inefficiencies in the corners of the base of the triangle.

For each collection of points, the track fit was performed with an assumed positive and negative charge. The momentum resolution and charge misidentification rates were determined by studying the fitted track in each case which had the better χ^2 per degree of freedom. Figure 3 shows the momentum resolution as a function of muon momentum. The tracker achieves a resolution of better than 10% over the momentum range studied. Figure 4(a) shows the efficiency for reconstructing positive muons as a function of the initial muon momentum. The detector becomes fully efficient above 400 MeV.

The charge misidentification rate was determined by counting the rate at which the track fit with the incorrect charge had a better χ^2 per degree of freedom than that with the correct charge. Figure 4(b) shows the charge misidentification rate as a function of the initial muon momentum.

The neutrino interactions were also reconstructed using the aid of the Monte Carlo information for pattern recognition. In an attempt to produce some of the effects of a real pattern recognition algorithm on the detector performance, only every fourth hit was collected for track fitting. Tracks were only fit if 10 such hits were found from a given particle. The Monte Carlo positions were smeared (Gaussian smearing using the 4.5 mm rms determined previously) and passed to the Kalman track fit. The reconstruction returned the following:

(i) the total momentum vector of all fitted tracks,
(ii) the momentum vector of the muon [muon ID from Monte Carlo truth],
(iii) the reconstructed and truth energy sum of all the hits that were not in a particle that was fitted, and
(iv) the reconstructed energy sum of all hits in the event.

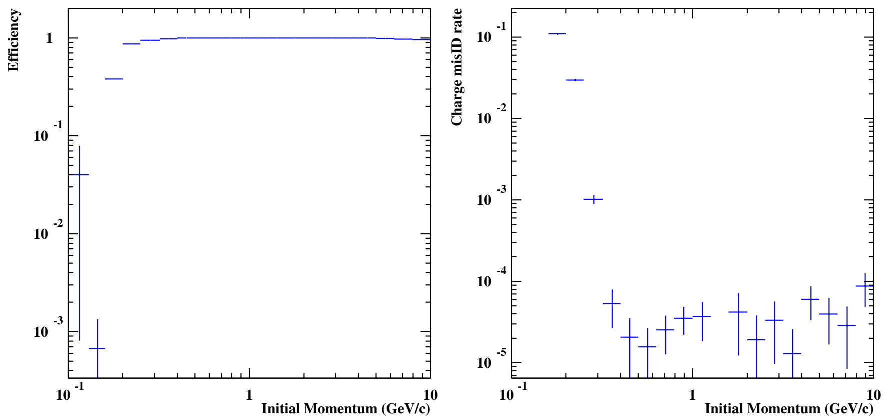

(a) (b)

FIG. 4 (color online). (a) Efficiency for reconstructing positive muons. (b) Muon charge misidentification rate as a function of the initial muon momentum.

The ν_μ CC event reconstruction efficiency as a function of neutrino energy is shown in Fig. 5(a). The fraction of ν_μ CC events with a reconstructed muon is shown in Fig. 5(b). In this figure the bands represent the limits of the statistical errors for this analysis.

Based on these initial neutrino factory TASD studies, in our phenomenological analysis we assume the detector has an effective threshold for measuring muon-neutrino CC events at $E_\nu = 500$ MeV, above which it has an energy independent efficiency of 73%. The 73% efficiency is primarily driven by the neutrino interaction kinematics, not by the detector tracking efficiency. No charge-ID criterion is applied here. The charge misidentification rate information is used as input into the effect of backgrounds on the analysis.

We note that to fully understand the backgrounds in the TASD requires a simulation that includes neutrino interactions and a full event reconstruction. Although this is beyond the scope of the present study, a consideration of backgrounds in the well-studied Magnetized Fe-Scintillator detector proposed for the high-energy neutrino factory [18] and The International Scoping Study for a Neutrino Factory [28] motivates the 10^{-3} background (contamination) assumption used in this paper for the TASD. Before kinematic cuts, the main backgrounds for the Fe-Scintillator detector are muon charge misidentification, charm decay, pion and kaon decay, and are all of comparable order: $1–5 \times 10^{-4}$. For the TASD at a low-energy neutrino factory the muon charge misidentification rate [Fig. 4(b)] and the charm decay background is suppressed (at the level $4–8 \times 10^{-5}$) due to the low-energy beam. Pion and kaon decay in flight become the main background concerns at the $1–5 \times 10^{-4}$ level. A figure of merit for comparing the TASD to a conventional

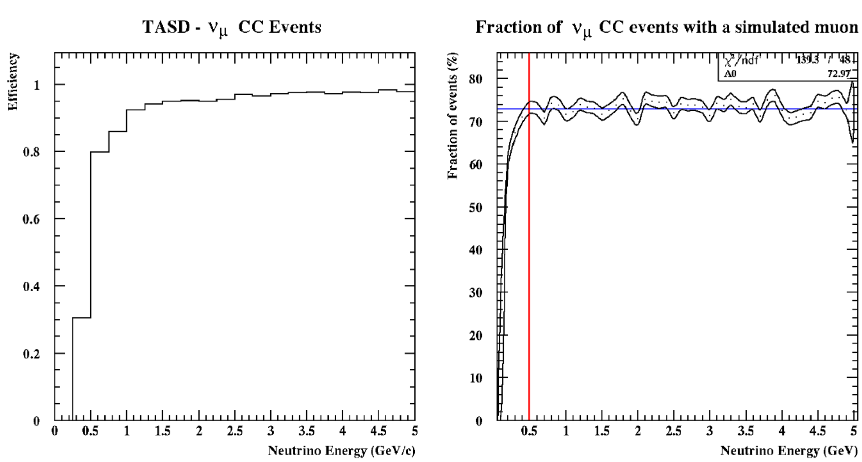

(a) (b)

FIG. 5 (color online). (a) Reconstruction efficiency of ν_μ CC events as a function of neutrino interaction energy. (b) Fraction of ν_μ CC events with a reconstructed muon.

Magnetized Fe-Scintillator detector is the ratio of their respective particle decay lengths to interaction lengths. For TASD the ratio is about 1; for the Magnetized Fe-Scintillator detector it is approximately 8. So naively we can conclude that the decay background in TASD will be 10 times worse than in the conventional detector ignoring any kinematic or topological cuts. However the TASD will have vastly superior kink detection to identify decay in flight. For example we will typically have 40 hits on the pion track before decay. In addition TASD will have continuous dE/dx measurements along the track and better overall energy resolution. We believe that these properties will allow us to control backgrounds to the 10^{-3} level or better.

III. PHYSICS REACH OF THE LOW-ENERGY NEUTRINO FACTORY

We have previously mentioned that, by exploiting the energy dependence of the signal, it is possible to extract from the measurements the correct values of θ_{13} and δ, and eliminate the additional solutions arising from discrete ambiguities. In the present study, we include the detector simulation results described in the previous section, which suggests a lower energy threshold (500 MeV) than previously assumed [26], and an energy resolution $dE/E = 30\%$.[2] Above threshold, the detector efficiency for muon-neutrino CC events is taken to be 73%.

In the following we consider the representative baseline $L = 1480$ km, which corresponds to the distance from Fermilab to the Henderson mine. However, we believe that the TASD will not require operation deep underground in order to remove backgrounds. Results are similar for other baselines in the 1200–1500 km range. The results are presented for the high-statistics scenario described in [26] as well as for a more aggressive scenario which improves the statistics of the old high-statistics scenario by a factor of 3, to quantify the benefits of increased detector sizes and/or stored-muon luminosities. The high-statistics scenario corresponds to 1×10^{23} kton decays (10 years of data taking, with 5×10^{20} useful muon decays of each sign per year, and a detector fiducial mass times efficiency of 20 kton). The more aggressive scenario corresponds to 3×10^{23} kton decays (which could correspond, for instance, to 10 years of data taking, with 1×10^{21} useful muon decays of each sign per year, and a detector fiducial mass times efficiency of 30 kton).

Table I shows the number of CC muon events expected in the two scenarios explored here for, respectively, the positive and negative muons stored in the neutrino factory. Notice that, in the absence of oscillations, there would be a few times 10^4 ν_e CC interactions, which would allow a search for $\nu_e \rightarrow \nu_\mu$ oscillations with probabilities below 10^{-4}.

All numerical results reported in the next sections have been obtained with the exact formulas for the oscillation probabilities. Unless specified otherwise, we take the following central values for the remaining oscillation parameters: $\sin^2\theta_{12} = 0.29$, $\Delta m^2_{21} = 8 \times 10^{-5}$ eV^2, $|\Delta m^2_{31}| = 2.5 \times 10^{-3}$ eV^2 and $\theta_{23} = 40°$. We show in Tables II and III, for two representative values of $\theta_{13} = 1°$ and $8°$, and the CP phase $\delta = 0°, 90°, 180°$ and $270°$, the number of wrong-sign muon events in the two scenar-

[2]We have assumed a very conservative $dE/E = 30\%$ because at this time the simulation work has not yet produced a number for the TASD. Based on NOνA results, we expect the TASD dE/E to be better than 6% at 2 GeV.

TABLE I. Neutrino and antineutrino charged currents interaction rates for $L = 1480$ km, for the 10^{23} kton-decay and the 3×10^{23} kton-decay statistics scenarios.

		μ^+		μ^-	
$E_{\mu^\mp} = 4.12$ GeV		$N_{\bar\nu_\mu}/10^3$	$N_{\nu_e}/10^3$	$N_{\nu_\mu}/10^3$	$N_{\bar\nu_e}/10^3$
Statistics	1	13	22	25	11
(10^{23}) kton decay	3	39	66	77	34

TABLE II. Wrong-sign muon event rates for normal (inverted) hierarchy, assuming $\nu_e \rightarrow \nu_\mu$ ($\bar\nu_e \rightarrow \bar\nu_\mu$) oscillations in a 20 kton fiducial volume detector, for a $L = 1480$ km baseline. We assume here $\theta_{13} = 8°$, i.e. $\sin^2 2\theta_{13} \simeq 0.076$. We present the results for several possible values of the CP-violating phase δ for both scenarios.

Statistics (kton decays)	$\delta(°)$	μ^+ stored (wrong sign: μ^-)	μ^- stored (wrong sign: μ^+)
1×10^{23}	0	880 (340)	180 (520)
	90	1230 (505)	90 (330)
	180	1000 (340)	170 (440)
	270	645 (175)	260 (625)
3×10^{23}	0	2640 (1020)	540 (1550)
	90	3700 (1520)	270 (990)
	180	2990 (1020)	510 (1310)
	270	1930 (520)	780 (1870)

TABLE III. As Table II but for $\theta_{13} = 1°$, i.e. $\sin^2 2\theta_{13} \simeq 0.001$.

Statistics (kton decays)	$\delta(°)$	μ^+ stored (wrong sign: μ^-)	μ^- stored (wrong sign: μ^+)
1×10^{23}	0	54 (50)	27 (37)
	90	100 (70)	13 (10)
	180	67 (50)	70 (25)
	270	22 (30)	37 (50)
3×10^{23}	0	160 (150)	80 (110)
	90	300 (210)	40 (30)
	180	200 (150)	230 (250)
	270	65 (90)	110 (150)

ios explored here, for, respectively, the positive and negative muons stored in the neutrino factory, for normal (inverted) hierarchy.

For our analysis, we use the following χ^2 definition:

$$\chi^2 = \sum_{i,j} \sum_{p,p'} (n_{i,p} - N_{i,p}) C^{-1}_{i,p:,j,p'} (n_{j,p'} - N_{j,p'}), \quad (3.1)$$

where $N_{i,\pm}$ is the predicted number of muons for a certain oscillation hypothesis, $n_{i,p}$ are the simulated "data" from a Gaussian or Poisson smearing and C is the $2N_{\rm bin} \times 2N_{\rm bin}$ covariance matrix given by

$$C^{-1}_{i,p:,j,p'} \equiv \delta_{ij} \delta_{pp'} (\delta n_{i,p})^2 \quad (3.2)$$

where $(\delta n_{i,p}) = \sqrt{n_{i,p} + (f_{\rm sys} \cdot n_{i,p})^2}$ contains both statistical and a 2% overall systematic error ($f_{\rm sys} = 0.02$).

A. Exploring the disappearance channel

Consider first the disappearance channels, already considered in the context of neutrino factories [17,56] and carefully explored in Ref. [57]. In Ref. [26] it was shown that, with its high statistics and good energy resolution, a low-energy neutrino factory can be used to precisely determine the atmospheric neutrino oscillation parameters, θ_{23} and Δm^2_{31}. In particular, for an exposure of 3×10^{22} kton decays for each muon sign, and allowing for a 2% systematic uncertainty, it was shown that (i) maximal mixing in the 23-sector could be excluded at 99% confidence level (C.L.) if $\sin^2\theta_{23} < 0.48$ ($\theta_{23} < 43.8°$), independently of the value of θ_{13}, and (ii) for a large value of θ_{13}, i.e. $\theta_{13} > 8°$, the θ_{23}-octant degeneracy would be resolved at the 99% C.L. for $\sin^2\theta_{23} < 0.44$ ($\theta_{23} < 41.5°$). In our present study, the good energy resolution of the TASD provides sensitivity to the oscillatory pattern of the disappearance signal that is comparable to, and somewhat better than, we previously assumed.

In Fig. 6 we show the 68%, 90% and 95% C.L. contours (for 2 dof) resulting from the fits to the measured energy dependent ν_μ and $\bar{\nu}_\mu$ CC rates at $L = 1480$ km. Results correspond to 1×10^{23} kton decays, and are shown for $\Delta m^2_{31} = 2.5 \times 10^{-3}$ eV^2 and two simulated values of $\sin^2\theta_{23}$ (= 0.4 and 0.44). For $\theta_{13} = 0$, $P_{\nu_\mu \to \nu_\mu}(\theta_{23}) = P_{\nu_\mu \to \nu_\mu}(\pi/2 - \theta_{23})$, i.e. the disappearance channel is symmetric under $\theta_{23} \to \pi/2 - \theta_{23}$. However, when a rather large nonvanishing value of θ_{13} is switched on, a θ_{23} asymmetry appears in the $P_{\nu_\mu \to \nu_\mu}$. Notice that the asymmetry grows with increasing θ_{13} and the fourfold degeneracy in the atmospheric neutrino parameters is resolved more easily. We conclude that, using only the ν_μ-disappearance data, the uncertainty on Δm^2_{31} could be reduced down to the 1%–2% level. In principle, the ν_e disappearance channel could also be used, which is sensitive to θ_{13} and matter effects. However, charge discrimination for electrons has not yet been adequately studied to determine the relevant TASD performance parameters.

The extremely good determination of the atmospheric mass squared difference opens the possibility to determine the mass hierarchy by exploiting the effects of the solar mass squared difference on the ν_μ disappearance probability, even for negligible values of θ_{13}. This strategy was studied in detail in Refs. [58–60]. The vacuum $\nu_\mu \to \nu_\mu$ oscillation probability is given by

$$\begin{aligned} P(\nu_\mu \to \nu_\mu) = 1 &- 4|U_{\mu 1}|^2 |U_{\mu 2}|^2 \sin^2 \frac{\Delta m^2_{12} L}{4E} \\ &- 4|U_{\mu 1}|^2 |U_{\mu 3}|^2 \sin^2 \frac{\Delta m^2_{13} L}{4E} \\ &- 4|U_{\mu 2}|^2 |U_{\mu 3}|^2 \sin^2 \frac{\Delta m^2_{23} L}{4E}, \end{aligned} \quad (3.3)$$

where the usual notation is used for the mass squared differences Δm^2_{ij} and for the elements of the leptonic mixing matrix U. In the following we take $\theta_{13} = 0$. The

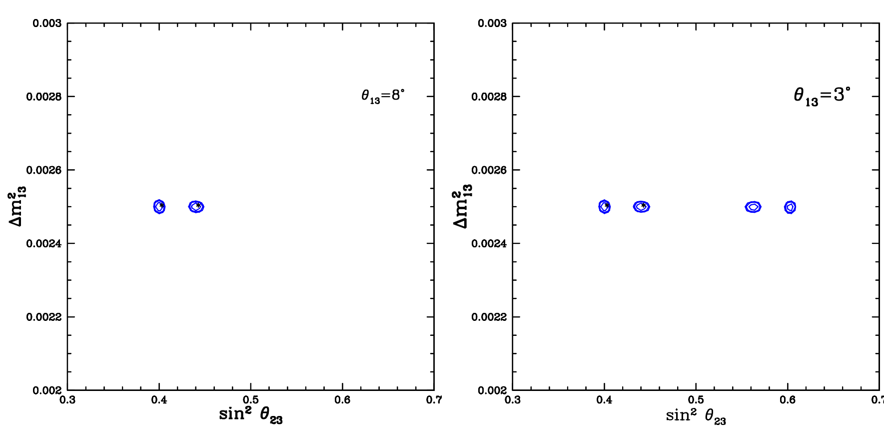

FIG. 6 (color online). 68%, 90% and 95% (2 dof) C.L. contours resulting from the fits at $L = 1480$ km assuming two central values for $\sin^2\theta_{23} = 0.4$ and 0.44 and $\Delta m^2_{31} = 2.5 \times 10^{-3}$ eV^2. In the left (right) panel, $\theta_{13} = 8°$ (3°). The statistics considered for both simulations corresponds to 1×10^{23} kton decays. Only disappearance data have been used to perform these plots.

oscillation probabilities depend on whether $|\Delta m^2_{13}| > |\Delta m^2_{23}|$ (normal hierarchy) or $|\Delta m^2_{13}| < |\Delta m^2_{23}|$ (inverted hierarchy). Precisely measured disappearance probabilities can distinguish between normal and inverted hierarchies if there is sensitivity to effects driven by both $|\Delta m^2_{13}|$ and Δm^2_{12}. This requires the atmospheric mass squared difference to be measured at different L/E with a precision of better than $|\Delta m^2_{21}|/|\Delta m^2_{31}| \sim 0.026$. In fact, it was pointed out in Ref. [58] that, for a fixed L/E, the disappearance probabilities for the normal and inverted hierarchies are the same if $|\Delta m^2_{13}|$ is substituted with

$$-|\Delta m^2_{13}| + \Delta m^2_{12} + \frac{4E}{L}\arctan\left(\cos 2\theta_{12}\tan\frac{\Delta m^2_{12}L}{4E}\right).$$

In order to break this degeneracy it is necessary to measure the atmospheric mass squared difference at different energies and at distances for which the oscillations driven by the solar term are non-negligible. In our setup, if we assume a 0% (2%) overall systematic error, we find that the hierarchy can be measured at the 1σ level (1σ level) for the 10^{23} kton-decay case, while for the 3×10^{23} kton-decay scenario it can be determined at the 4σ level (2σ level). Note that the systematic errors play a crucial role. It is in principle possible to reduce the impact of the systematics errors using the ratios of the number of events at the near and far detectors:

$$\mathcal{R}(E) = \frac{\frac{N_{\rm N}(\nu_\mu)}{N_{\rm N}(\bar{\nu}_e)}}{\frac{N_{\rm F}(\nu_\mu)}{N_{\rm F}(\bar{\nu}_e)}}, \qquad (3.4)$$

where $N_{\rm N(F)}(\nu_\mu[\bar{\nu}_e])$ refer to the number of $\nu_\mu[\bar{\nu}_e]$ events in the near (far) detector for a fixed energy E. Very good energy resolution is required for such cancellations to be effective. In this case, a low-energy neutrino factory can give important information on the type of hierarchy even if $\theta_{13} = 0$.

B. Simultaneous fits to θ_{13} and δ

Next, we study the extraction of the unknown parameters θ_{13} and δ, using the golden channel $[\nu_e(\bar{\nu}_e) \to \nu_\mu(\bar{\nu}_\mu)]$. We start by considering a neutrino factory scenario with 1×10^{23} kton decays. We find that, for values of $\theta_{13} > 2°$, the sign degeneracy is resolved at the 95% C.L. Note that for $\theta_{13} > 4°$ the octant degeneracy has already been resolved using the disappearance data.

Figure 7 shows, for a fit to the simulated data at a baseline $L = 1480$ km, the 68%, 90% and 95% C.L. contours in the (θ_{13}, δ)-plane. Results are shown for background levels set to zero (left panel) and 10^{-3} (right panel) for the 10^{23} kton-decay scenario. The four sets of contours correspond to four simulated test points in the (θ_{13}, δ)-plane, which are depicted by a star. The simulations are for the normal mass hierarchy and θ_{23} in the first octant ($\sin^2\theta_{23} = 0.41$ which corresponds to $\theta_{23} = 40°$). Our analysis includes the study of the discrete degeneracies. That is, we have fitted the data assuming both the right and wrong hierarchies, and the right and wrong choices for the θ_{23} octant. If present, the additional solutions associated to the θ_{23} octant ambiguity are shown as dotted contours.

Notice from Fig. 7 that the sign ambiguity is resolved at the 95% C.L. in the 10^{23} kton-decay scenario. Additional solutions associated to the wrong choice of the θ_{23} octant are still present in the 10^{23} kton-decay scenario, but notice that the presence of these additional solutions does not interfere with a measurement of the CP violating phase δ and θ_{13}, since the locations of the fake solutions in the (θ_{13}, δ) plane are almost the same as the correct locations.

The effect of the background can be easily understood in terms of the statistics presented in Tables II and III. For

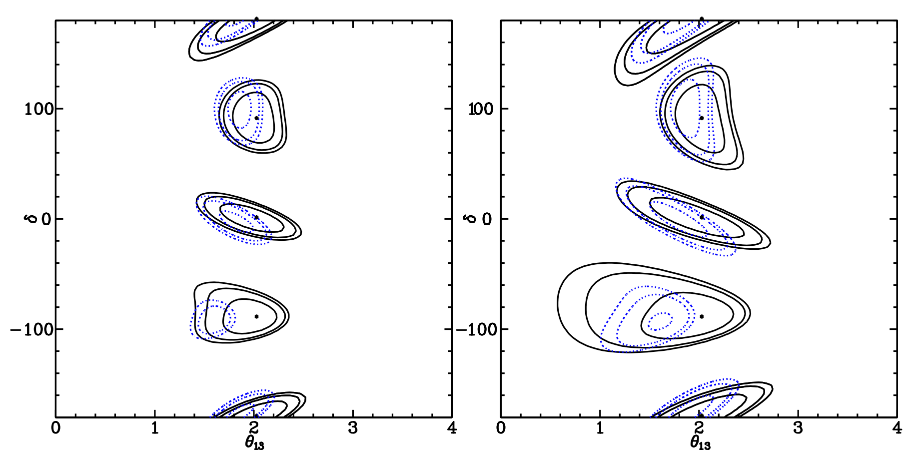

FIG. 7 (color online). 68%, 90% and 95% (2 dof) C.L. contours resulting from the fits at $L = 1480$ km assuming four central values for $\delta = 0°, 90°, -90°$ and $180°$ and $\theta_{13} = 2°$ without backgrounds (left panel) and with a background level of 10^{-3} (right panel). The additional θ_{23} octant solutions are depicted by dotted lines. The statistics considered for both simulations corresponds to 10^{23} kton decays.

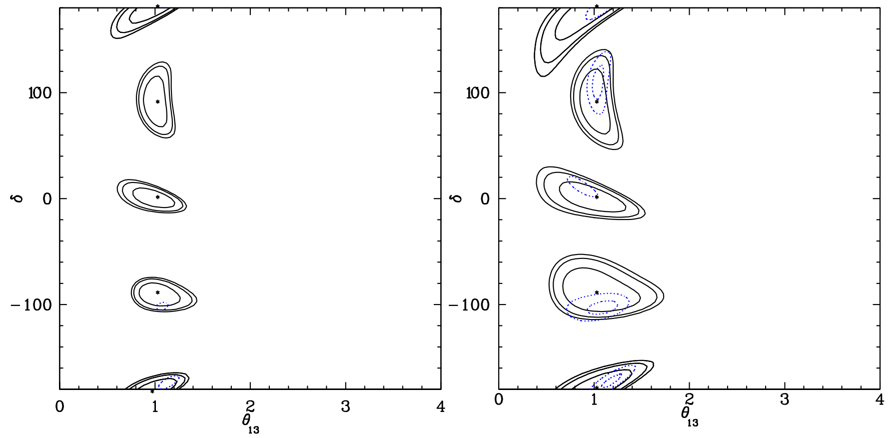

FIG. 8 (color online). 68%, 90% and 95% (2 dof) C.L. contours resulting from the fits at $L = 1480$ km assuming four central values for $\delta = 0°, 90°, -90°$ and $180°$ and $\theta_{13} = 1°$ without backgrounds (left panel) and with a background level of 10^{-3} (right panel). The statistics considered for both simulations correspond to 3×10^{23} kton decays.

small values of θ_{13}, the addition of the background has a larger impact for $\delta \sim -90°$, since for that value of the *CP* phase the statistics are dominated by the antineutrino channel, which suffers from a larger background (from ν_μ's) than the neutrino channel (from $\bar{\nu}_\mu$'s). For a background level smaller than $\sim 10^{-4}$, the results are indistinguishable from the zero background case.

We illustrate the corresponding results for the improved scenario of 3×10^{23} kton decays in Fig. 8. Note that the higher statistics allow us to consider a smaller value for $\theta_{13} = 1°$. The additional solutions arising from the wrong choice for the neutrino mass hierarchy or θ_{23} octant are not present at the 95% C.L. Furthermore, the addition of a background level of 10^{-3} does not significantly affect the resolution of the degeneracies, and has only an impact on the *CP* violation measurement.

The performance of the *low-energy neutrino factory* in the two high-statistics scenarios explored here is unique. The sign (Δm^2_{31}) can be determined at the 95% C.L. in the 10^{23} kton-decay (3×10^{23} kton-decay) scenario if $\theta_{13} > 2°$ ($> 1°$) for all values of the *CP* phase δ. The θ_{23}-octant ambiguity can be removed at the 95% C.L. down to roughly $\theta_{13} > 0.5 - 1.0°$ for the representative choice of $\sin^2\theta_{23} = 0.41$, independently of the value of δ, except for some intermediate values of $\theta_{13} \sim 2°$, for which the θ_{23} degeneracy is still present for some values of the *CP* violating phase δ. Resolving the θ_{23}-octant degeneracy therefore is easier for small values of $\theta_{13} < 2°$. This is due to the fact that, as explored in Ref. [26], the θ_{23}-octant degeneracy is resolved using the information from the low-energy bins, which are sensitive to the solar term. For the setup described in this paper, the solar term starts to be important if $\theta_{13} < 2°$. However, notice that the presence of the θ_{23} octant ambiguity at $\theta_{13} \sim 2°$ will not interfere with the extraction of θ_{13} and δ, since the locations of the degenerate (fake) solutions almost coincide with the positions of "true," nature solutions.

In Figs. 9 and 10 we summarize, for the 10^{23} and 3×10^{23} kton-decay scenarios, the physics reach for a TASD detector located 1480 km from a low-energy neutrino factory. The analysis takes into account the impact of both the intrinsic and discrete degeneracies. Figure 9 shows the region in the ($\sin^2 2\theta_{13}$, "fraction of δ") plane for which the mass hierarchy can be resolved at the 95% C.L. (1 dof). Contours are shown for zero background, and for when a background level of 10^{-3} is included in the

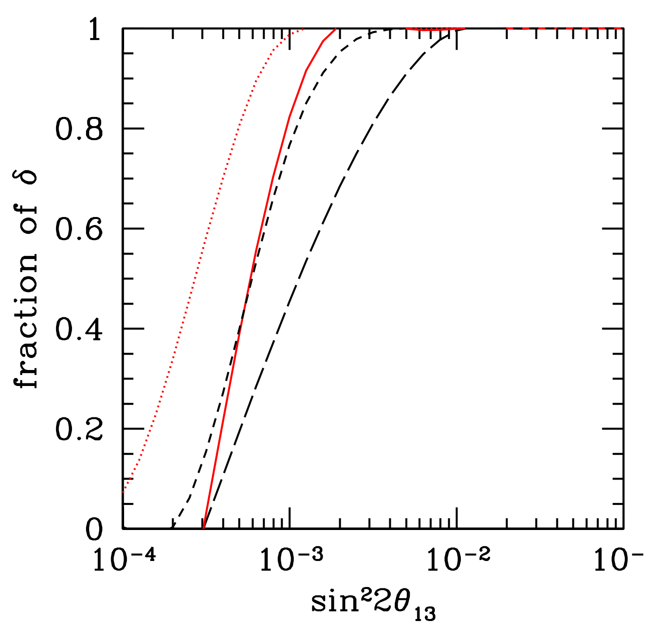

FIG. 9 (color online). 95% C.L. (1 dof) hierarchy resolution assuming that the far detector is located at a distance of 1480 km at the Henderson mine. The solid (dotted) curves depict the results assuming 1×10^{23} kton decays (3×10^{23} kton decays) without backgrounds. The long-dashed (short-dashed) black curves depict the results assuming 1×10^{23} kton decays (3×10^{23} kton decays) with a background level of 10^{-3}.

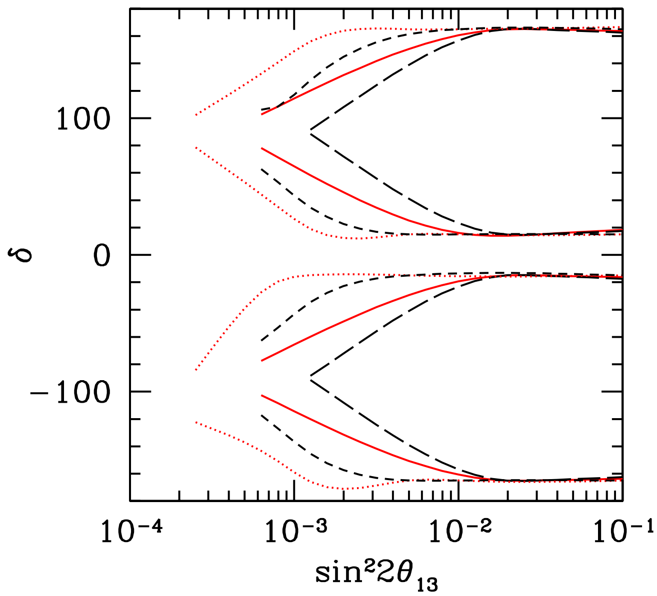

FIG. 10 (color online). 95% C.L. (1 dof) CP violation extraction assuming that the far detector is located at a distance of 1480. The solid (dotted) curves depict the results assuming 1×10^{23} kton decays (3×10^{23} kton decays) without backgrounds. The long-dashed (short-dashed) black curves depict the results assuming 1×10^{23} kton decays (3×10^{23} kton decays) with a background level of 10^{-3}.

analysis. Note that, with a background level of $\simeq 10^{-3}$, the hierarchy can be determined in both scenarios if $\sin^2 2\theta_{13} >$ few 10^{-3} (i.e. $\theta_{13} > 2$–$3°$) for all values of the CP violating phase δ. For a background level smaller than $\sim 10^{-4}$, the results are indistinguishable from the zero background case.

Figure 10 shows the region in the ($\sin^2 2\theta_{13}$, δ) plane for which a given (nonzero) CP violating value of the CP-phase δ can be distinguished at the 95% C.L. (1 dof) from the CP conserving case, i.e. $\delta = 0, \pm 180°$. The results are given for the two statistics scenarios studied here. Note that, even in the presence of a 10^{-3} background level, the CP violating phase δ could be measured with a 95% C.L. precision of better than 20° in the 10^{23} kton-decay (3×10^{23} kton-decay) luminosity scenario if $\sin^2 2\theta_{13} > 0.01$ ($\sin^2 2\theta_{13} > 0.002$).

IV. SUMMARY AND CONCLUSIONS

We have studied the physics reach of a low-energy neutrino factory, first presented in Ref. [26], in which the stored muons have an energy of 4.12 GeV. The simulated detector performance is based upon a magnetized totally active scintillator detector. Our simulations suggest this detector will have a threshold for measuring muon-neutrino CC interactions of about 500 MeV and an energy independent efficiency of about 73% above threshold. We have assumed a conservative energy resolution of 30% for the detector.

In our analysis, we consider the representative baseline of 1480 Km, divide the simulated observed neutrino event spectrum into 9 energy bins above the 500 MeV threshold, and exploit both the disappearance ($\nu_\mu \to \nu_\mu$) and the golden ($\nu_e \to \nu_\mu$) channels by measuring CC events tagged by right-sign and wrong-sign muons. The results can be easily generalized to other baselines in the 1200–1500 km range. We have investigated the dependence of the physics sensitivity on statistics by considering a high-statistics scenario corresponding to 1×10^{23} kton decay for each muon sign, and a more aggressive scenario corresponding to 3×10^{23} kton decay for each muon sign. We have also explored the impact of backgrounds to the wrong-sign muon signal by considering background levels of zero and 10^{-3}.

We find that, based only on the disappearance channel, maximal atmospheric neutrino mixing can be excluded at 95% C.L. if $\sin^2\theta_{23} < 0.44$ ($\theta_{23} < 41.5°$). The atmospheric mass difference could be measured with a precision of 1%–2%, opening the possibility of determining the neutrino mass hierarchy even if $\theta_{13} = 0$, provided systematic uncertainties can be controlled. Neglecting systematic uncertainties, the mass hierarchy could be determined at the 1σ level (4σ level) in the 1×10^{23} kton-decay (3×10^{23} kton-decay) statistics scenario.

The rich oscillation pattern of the $\nu_e \to \nu_\mu$ ($\bar{\nu}_e \to \bar{\nu}_\mu$) appearance channels at energies between 0.5 and 4 GeV for baselines $\mathcal{O}(1000)$ km facilitates an elimination of the degenerate solutions. If the atmospheric mixing angle is not maximal, for the representative choice of $\sin^2\theta_{23} = 0.4$, the octant in which θ_{23} lies could be extracted at the 95% C.L. in both scenarios if $\theta_{13} > 0.5 - 1°$, for all values of the CP violating phase δ, except for some intermediate values of the mixing angle θ_{13} in which the fake solutions's location coincides with the true solution's position and therefore the presence of these fake solutions does not interfere with the extraction of δ_{CP} and θ_{13}.

In the 10^{23} kton-decay scenario, if the background level is $\sim 10^{-3}$ (10^{-4}), the neutrino mass hierarchy could be determined at the 95% C.L., and the CP violating phase δ could be measured with a 95% C.L. precision of better than 20°, if $\sin^2 2\theta_{13} > 0.01$ (~ 0.006). With a factor of 3 improvement in the former statistics, the numbers quoted above are $\sin^2 2\theta_{13} = 0.005$ and $\sin^2 2\theta_{13} = 0.002$, for background levels of 10^{-3} and 10^{-4}, respectively. In our analysis we have included a 2% systematic error on all measured event rates.

In summary, the low statistics low-energy neutrino factory scenario we have described, with a background level of 10^{-3}, for both large and very small values of θ_{13} would be able to eliminate ambiguous solutions, determine θ_{13}, the mass hierarchy, and search for CP violation. Higher statistics and lower backgrounds would further improve the sensitivity, and may enable the mass hierarchy to be determined even if $\theta_{13} = 0$.

ACKNOWLEDGMENTS

This work was supported in part by the European Programme "The Quest for Unification" Contract No. MRTN-CT-2004-503369, and by the Fermi National Accelerator Laboratory, which is operated by the Fermi Research Association, under Contract No. DE-AC02-76CH03000 with the U.S. Department of Energy. S. P. acknowledges the support of CARE, Contract No. RII3-CT-2003-506395. O. M. and S. P. would like to thank the Theoretical Physics Department at Fermilab for hospitality and support.

APPENDIX

All detector concepts for the neutrino factory require a magnetic field in order to determine the sign of muon (or possibly the electron) produced in the neutrino interaction. For the baseline detector, this is done with magnetized iron. Technically this is very straightforward, although the 100 kton baseline detector does present challenges because of its size. The cost of this magnetic solution is felt to be manageable. Magnetic solutions for the TASD become much more problematic. The solution that we propose is to use the STL developed for the VLHC [53], Fig. 1, as

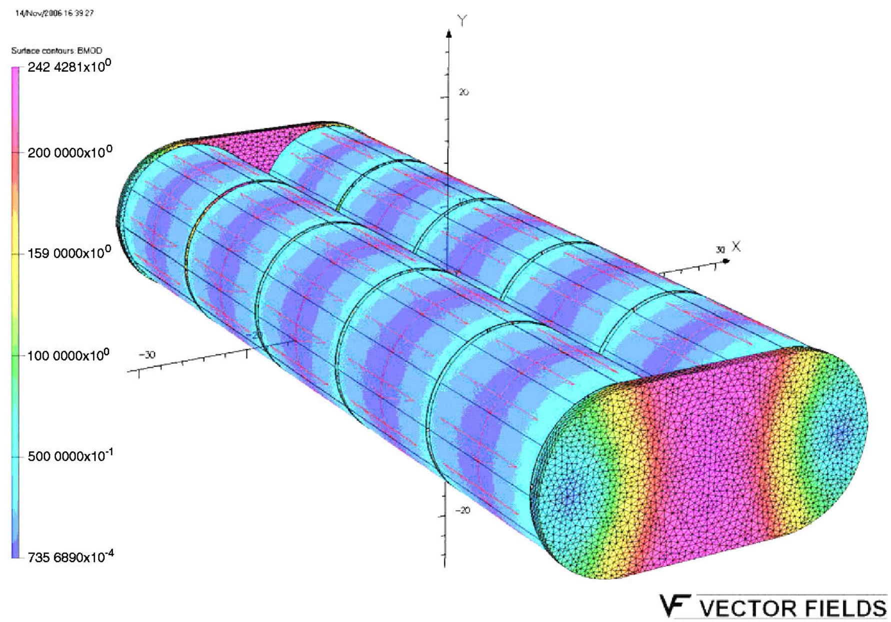

FIG. 11 (color online). Simulation results for magnetic cavern design.

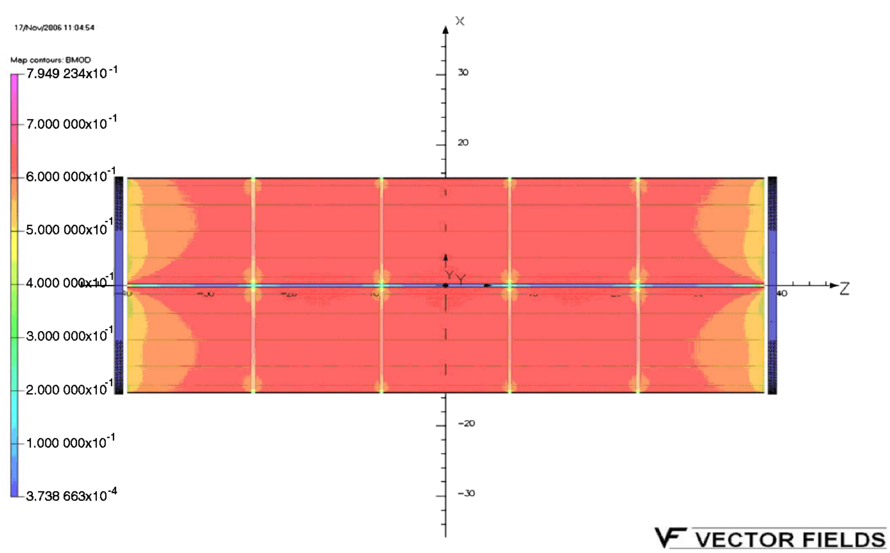

FIG. 12 (color online). STL solenoid magnetic cavern field uniformity in the X-Z plane.

windings for very large solenoids that form a magnetic cavern (see Fig. 11) for the detector. The STL consists of a superconducting cable inside a cryopipe cooled by supercritical liquid helium at 4.5–6.0 K placed inside a coaxial cryostat. It consists of a perforated Invar tube, a copper stabilized superconducting cable, an Invar helium pipe, the cold pipe support system, a thermal shield covered by multilayer superinsulation, and the vacuum shell. One of the possible STL designs developed for the VLHC is shown in Fig. 11 within the main text. The STL is designed to carry a current of 100 kA at 6.5 K in a magnetic field up to 1 T. This provides a 50% current margin with respect to the required current in order to reach a field of 0.5 T. This operating margin can compensate for temperature variations, mechanical or other perturbations in the system.

The solenoid windings now consist of this superconducting cable which is confined in its own cryostat. Each solenoid consists of 150 turns and requires ~7500 m of cable. There is no large vacuum vessel and access to the detectors can be made through the winding support cylinder since the STL does not need to be close packed in order to reach an acceptable field. We have performed a simulation of the magnetic cavern concept using STL solenoids and the results are shown in Fig. 12. With the iron end walls (1 m thick), the average field in the X-Z plane is approximately 0.58 T at an excitation current of 50 kA. This figure shows the field uniformity in the X-Z plane which is better than $\pm 2\%$ throughout the majority of the volume with approximately 20% variations near the end irons. Figure 13 shows the on-axis B field as a function of position along the z axis (in meters).

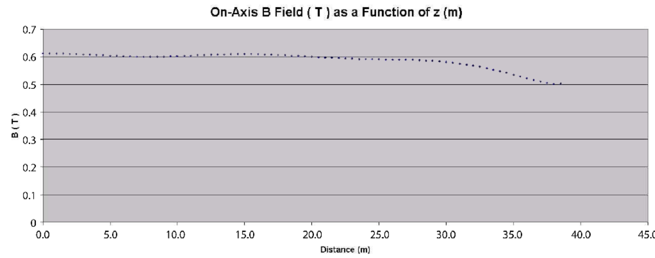

FIG. 13 (color online). On-axis B field in T as a function of position along the z axis (m).

We have not yet been able to do a detailed costing of the magnetic cavern. The STL costs can be estimated quite accurately (30%) from the VLHC work and current superconducting cable costs and are believed to be 50 M. The total magnetic cavern cost is estimated to be less than 150 M. This is to be compared to a fully loaded cost savings of the low-energy neutrino factory (compared to the 50 GeV design) as indicated in Ref. [28].-

[1] Y. Ashie *et al.* (Super-Kamiokande Collaboration), Phys. Rev. D **71**, 112005 (2005).
[2] B. T. Cleveland *et al.*, Astrophys. J. **496**, 505 (1998); Y. Fukuda *et al.* (Kamiokande Collaboration), Phys. Rev. Lett. **77**, 1683 (1996); J. N. Abdurashitov *et al.* (SAGE Collaboration), J. Exp. Theor. Phys. **95**, 181 (2002); W. Hampel *et al.* (GALLEX Collaboration), Phys. Lett. B **447**, 127 (1999); T. A. Kirsten *et al.* (GNO Collaboration), Nucl. Phys. B, Proc. Suppl. **118**, 33 (2003).
[3] S. Fukuda *et al.* (Super-Kamiokande Collaboration), Phys. Lett. B **539**, 179 (2002).
[4] Q. R. Ahmad *et al.* (SNO Collaboration), Phys. Rev. Lett. **87**, 071301 (2001).
[5] Q. R. Ahmad *et al.* (SNO Collaboration), Phys. Rev. Lett. **89**, 011301 (2002); **89**, 011302 (2002).
[6] S. N. Ahmed *et al.* (SNO Collaboration), Phys. Rev. Lett. **92**, 181301 (2004).
[7] B. Aharmim *et al.* (SNO Collaboration), Phys. Rev. C **72**, 055502 (2005).
[8] K. Eguchi *et al.* (KamLAND Collaboration), Phys. Rev. Lett. **90**, 021802 (2003).
[9] M. H. Ahn *et al.* (K2K Collaboration), Phys. Rev. D **74**, 072003 (2006).
[10] D. G. Michael *et al.* (MINOS Collaboration), Phys. Rev. Lett. **97**, 191801 (2006).
[11] T. Schwetz, Phys. Scr. **T127**, 1 (2006).
[12] G. L. Fogli *et al.*, Phys. Rev. D **75**, 053001 (2007).
[13] M. C. Gonzalez-Garcia and M. Maltoni, arXiv:0704.1800.
[14] S. Geer, Phys. Rev. D **57**, 6989 (1998); **59**, 039903(E) (1999).
[15] A. De Rujula, M. B. Gavela, and P. Hernandez, Nucl. Phys. **B547**, 21 (1999).
[16] V. D. Barger, S. Geer, and K. Whisnant, Phys. Rev. D **61**, 053004 (2000); A. Donini *et al.*, Nucl. Phys. **B574**, 23 (2000); V. D. Barger *et al.*, Phys. Rev. D **62**, 073002 (2000).
[17] V. D. Barger *et al.*, Phys. Rev. D **62**, 013004 (2000).
[18] A. Cervera *et al.*, Nucl. Phys. **B579**, 17 (2000); **B593**, 731 (E) (2001).
[19] M. Freund, P. Huber, and M. Lindner, Nucl. Phys. **B585**, 105 (2000); V. D. Barger *et al.*, Phys. Lett. B **485**, 379 (2000); J. Burguet-Castell *et al.*, Nucl. Phys. **B608**, 301 (2001); M. Freund, P. Huber, and M. Lindner, Nucl. Phys. **B615**, 331 (2001).
[20] A. Donini, D. Meloni, and P. Migliozzi, Nucl. Phys. **B646**, 321 (2002); D. Autiero *et al.*, Eur. Phys. J. C **33**, 243 (2004).
[21] C. Albright *et al.*, arXiv:hep-ex/0008064.
[22] A. Blondel *et al.*, Nucl. Instrum. Methods Phys. Res., Sect. A **451**, 102 (2000); M. Apollonio *et al.*, arXiv:hep-ph/0210192.
[23] C. Albright *et al.* (Neutrino Factory/Muon Collider Collaboration), arXiv:physics/0411123.
[24] O. Mena, Mod. Phys. Lett. A **20**, 1 (2005).

[25] P. Huber, M. Lindner, M. Rolinec, and W. Winter, Phys. Rev. D **74**, 073003 (2006).
[26] S. Geer, O. Mena, and S. Pascoli, Phys. Rev. D **75**, 093001 (2007).
[27] P. Huber and W. Winter, Phys. Lett. B **655**, 251 (2007).
[28] A. Bandyopadhyay *et al.* (ISS Physics Working Group), Report No. RAL-TR-2007-24.
[29] G. L. Fogli and E. Lisi, Phys. Rev. D **54**, 3667 (1996).
[30] H. Minakata and H. Nunokawa, J. High Energy Phys. 10 (2001) 001.
[31] V. D. Barger, S. Geer, R. Raja, and K. Whisnant, Phys. Rev. D **63**, 113011 (2001).
[32] T. Kajita, H. Minakata, and H. Nunokawa, Phys. Lett. B **528**, 245 (2002); H. Minakata, H. Nunokawa, and S. J. Parke, Phys. Rev. D **66**, 093012 (2002); P. Huber, M. Lindner, and W. Winter, Nucl. Phys. **B645**, 3 (2002); A. Donini, D. Meloni, and S. Rigolin, J. High Energy Phys. 06 (2004) 011; M. Aoki, K. Hagiwara, and N. Okamura, Phys. Lett. B **606**, 371 (2005); O. Yasuda, New J. Phys. **6**, 83 (2004); O. Mena and S. J. Parke, Phys. Rev. D **72**, 053003 (2005).
[33] H. Minakata and H. Nunokawa, Phys. Lett. B **413**, 369 (1997).
[34] V. Barger, D. Marfatia, and K. Whisnant, Phys. Rev. D **66**, 053007 (2002).
[35] O. Mena Requejo, S. Palomares-Ruiz, and S. Pascoli, Phys. Rev. D **72**, 053002 (2005).
[36] M. Ishitsuka *et al.*, Phys. Rev. D **72**, 033003 (2005); K. Hagiwara, N. Okamura, and K. i. Senda, Phys. Lett. B **637**, 266 (2006).
[37] O. Mena, S. Palomares-Ruiz, and S. Pascoli, Phys. Rev. D **73**, 073007 (2006).
[38] T. Kajita *et al.*, Phys. Rev. D **75**, 013006 (2007).
[39] J. Burguet-Castell *et al.*, Nucl. Phys. **B646**, 301 (2002).
[40] P. Huber, M. Lindner, and W. Winter, Nucl. Phys. **B654**, 3 (2003).
[41] H. Minakata, H. Nunokawa, and S. J. Parke, Phys. Rev. D **68**, 013010 (2003).
[42] V. Barger, D. Marfatia, and K. Whisnant, Phys. Lett. B **560**, 75 (2003).
[43] K. Whisnant, J. M. Yang, and B. L. Young, Phys. Rev. D **67**, 013004 (2003); P. Huber *et al.*, Nucl. Phys. **B665**, 487 (2003); P. Huber *et al.*, Phys. Rev. D **70**, 073014 (2004); A. Donini, E. Fernández-Martínez, and S. Rigolin, Phys. Lett. B **621**, 276 (2005).
[44] O. Mena and S. J. Parke, Phys. Rev. D **70**, 093011 (2004).
[45] P. Huber, M. Maltoni, and T. Schwetz, Phys. Rev. D **71**, 053006 (2005).
[46] S. Choubey and P. Roy, Phys. Rev. D **73**, 013006 (2006).
[47] A. Blondel *et al.*, Acta Phys. Pol. B **37**, 2077 (2006); A. Blondel, arXiv:hep-ph/0606111.
[48] O. Mena, H. Nunokawa, and S. J. Parke, Phys. Rev. D **75**, 033002 (2007); O. Mena, arXiv:hep-ph/0609031.
[49] D. Ayres *et al.*, arXiv:hep-ex/0503053.
[50] J. Hylen *et al.*, Report No. FERMILAB-TM-2018, 1997.
[51] K. S. McFarland, Eur. Phys. J. A **24S2**, 187 (2005).
[52] P. Baringer *et al.* (D0 Collaboration), Nucl. Instrum. Methods Phys. Res., Sect. A **469**, 295 (2001).
[53] Ambrosio *et al.*, Report No. Fermilab-TM-2149, 2001.
[54] D. Casper, Nucl. Phys. B, Proc. Suppl. **112**, 161 (2002).
[55] A. Cervera-Villanueva, J. J. Gomez-Cadenas, and J. A. Hernando, Nucl. Instrum. Methods Phys. Res., Sect. A **534**, 180 (2004).
[56] A. Bueno, M. Campanelli, and A. Rubbia, Nucl. Phys. **B589**, 577 (2000).
[57] A. Donini *et al.*, Nucl. Phys. **B743**, 41 (2006).
[58] A. de Gouvea, J. Jenkins, and B. Kayser, Phys. Rev. D **71**, 113009 (2005).
[59] A. de Gouvea and W. Winter, Phys. Rev. D **73**, 033003 (2006).
[60] H. Minakata, H. Nunokawa, S. J. Parke, and R. Zukanovich Funchal, Phys. Rev. D **74**, 053008 (2006).